From the grating scale monitor to the generalized seeing monitor

Aziz Ziad, Rodolphe Conan, Andrei Tokovinin, François Martin, and Julien Borgnino

An instrument named the grating scale monitor for measuring the outer scale $\mathscr{L}_0$ from the angle-of-arrival (AA) fluctuations of a perturbed wave front was developed a few years ago at Nice University. The AA is detected with a 5-ms time resolution by modulation of the stellar image in a small telescope with a grating. One uses the normalized covariance of AA fluctuations to estimate $\mathscr{L}_0$. A new version of this instrument, the generalized seeing monitor (GSM) is described. It consists of four identical modules for measuring the AA at four locations on the wave front. A spatiotemporal analysis of these data leads to the determination of seeing ϵ_0, outer scale $\mathscr{L}_0$, and the wave-front speed. In addition, isoplanatic angle θ_0 is determined from scintillation, making the characterization of turbulence with the GSM almost complete. We describe the instrument and make a detailed analysis of its performance and accuracy. Several site-testing campaigns have been conducted with the GSM: at La Silla (Chile), Oukaïmeden (Morocco), Maidanak (Uzbekistan), and Cerro Pachon and Cerro Paranal (Chile). The main results of these campaigns are presented and discussed.

OCIS codes: 010.1290, 010.1330, 010.1300, 010.1350, 010.1080.

1. Introduction

Advances in understanding the formation of astronomical images through the terrestrial atmosphere have made important contributions to improving the resolution of ground-based optical instruments. To optimize the performance of high-angular-resolution (HAR) techniques, e.g., those of adaptive optics (AO) and long-baseline interferometry (LBI), requires good knowledge of the atmospheric optical parameters (AOP's) related to the perturbed wave front.[1,2] Among these parameters are the well-known Fried diameter r_0, which is related to seeing angle $\epsilon_0 = 0.98\lambda/r_0$, isoplanatic angle θ_0, wave-front outer scale $\mathscr{L}_0$, and wave-front coherence time τ_0.

Many studies show the effect of finite $\mathscr{L}_0$ on the HAR techniques, but few measurements of this effect have been made so far.[3–5] In addition, the value of this outer scale parameter is controversial because the available measurements provide values scattered from a few meters to kilometers.[6] This optical parameter $\mathscr{L}_0$, also called the spatial coherence outer scale of the perturbed wave front, must be differentiated from the local outer scale $L_0(h)$ that depends on local conditions and so on altitude h.[7] $\mathscr{L}_0$ is defined as the distance at which the phase structure function saturates. $\mathscr{L}_0$ can also be interpreted as a combination of outer scales in different atmospheric layers weighted with the refractive-index structure constant profile $C_N^2(h)$.[8,9] The outer-scale values provided by the our grating-scale monitor correspond to the $\mathscr{L}_0$ parameter in the von Kármán model of the phase spectrum [Eq. (14) below]. Thus the $\mathscr{L}_0$ measured with the grating-scale monitor are model dependent, and the use of another model would change the outer scale values. The effect of the model on the $\mathscr{L}_0$ estimations is analyzed in Section 4 below.

The initial version of our instrument, the grating scale monitor, was intended for measurements of $\mathscr{L}_0$.[10] Recently some technical improvements and theoretical developments were made, and now it is possible to measure ϵ_0, $\mathscr{L}_0$, τ_0, and θ_0 with the grating scale monitor; Hence the name of the improved instrument is the generalized seeing monitor (GSM). For the first time to our knowledge, it is now possible to monitor the temporal evolution of the outer scale.

In Section 2 we describe the instrument and the data-reduction procedures. Then in Section 3 we analyze the measurement errors, including the influence of finite exposure time on the derived AOP.

A. Ziad (aziz.ziad@unice.fr), R. Conan, F. Martin, and J. Borgnino are with the Unité Mixte de Recherche Astrophysique 6525, Université de Nice-Sophia Antipolis, Parc Valrose, 06108 Nice Cedex 2, France. A. Tokovinin is with the Stenberg Astronomical Institute, Universitetsky Prospekt 13, 119899 Moscow, Russia.

Received 25 October 1999; revised manuscript received 1 June 2000.

0003-6935/00/305415-11$15.00/0

The dependence of $\mathscr{L}_0$ on the turbulence model used in the data reduction is investigated in Section 4 below. In addition, the methods that we used to estimate isoplanatic angle and wave-front speed are described in Sections 5 and 6, respectively. Finally, in Section 7 we give a summary of the measurement campaigns made with the GSM at five observatories.

2. Generalized Seeing Monitor Instrument

The GSM instrument consists of four identical modules, each module measuring the atmospheric angle-of-arrival (AA) fluctuations at selected positions on the wave front, as does a Shack–Hartmann sensor. We first describe the operation of an individual module. Then we describe the data-analysis procedure that we used to derive the atmospheric optical parameters.

A. Description of a Module

Each GSM module comprises a Maksutov telescope ($D = 100$ mm, $F = 1$ m) with a detector box. All four modules are pointed to the same star and are controlled by a single PC computer by means of a custom-made interface board. Modules 1 and 2 are installed on the same mount and act as a differential image-motion monitor.[11]

CCD detectors offer a standard way to measure the image position. However, the time needed to read the detector is still too long for fast and continuous monitoring of AA fluctuations. This is why we developed an alternative modulation technique for fast AA measurements in one direction.

The image of the observed star is formed upon a Ronchi grating. It is shifted by a galvanometric mirror manipulated by a 200-Hz triangular signal. The grating is scanned over one grating period (Fig. 1). The flux transmitted through the grating is detected by a photomultiplier working in the photon-counting mode. Four flux measurements per modulation period, which correspond to phase shifts 0, $\pi/2$, π, and $3\pi/2$, are taken. We denote the corresponding numbers of detected photons A, B, C, D (Fig. 1). If the flux modulation is sinusoidal, the phase Φ of this sinusoid can be calculated as[12]

$$\Phi = \frac{1}{2\pi} \tan^{-1}\left(\frac{D-B}{A-C}\right). \tag{1}$$

Modulation contrast γ is also estimated from the same A, B, C, and D fluxes as

$$\gamma = \frac{\pi^2}{2} \frac{(C-A)^2 + (D-B)^2}{(A+B+C+D)^2}. \tag{2}$$

Here we take into account the integration of the signal during the quarter-period when we accumulate the *ABCD* counts, so γ is the true contrast ($\gamma = 1$ for perfect sinusoidal modulation).

This technique is widely used for interferometric measurements[12] and is sometimes called the *ABCD* method (the term phase used here to denote image position was borrowed from interferometry). In Eq. (1) the phase is expressed in units of grating period. The AA is $\alpha = p\,\Phi$, where p is the angular period of the grating in radians or arcseconds ($p \approx 10$ arc sec for the GSM). If image motion exceeds one grating period, the integer number of periods can be restored by continuity, provided that the rapid fluctuations are less than $p/2$ (in practice this means that seeing must be better than $\approx$3 arc sec; otherwise phase jumps of one period may occur in the restored phases). The choice of the grating period is a compromise between AA measurement accuracy (which improves with decreasing p) and the necessity to have high-contrast modulation without phase jumps even for relatively poor seeing.

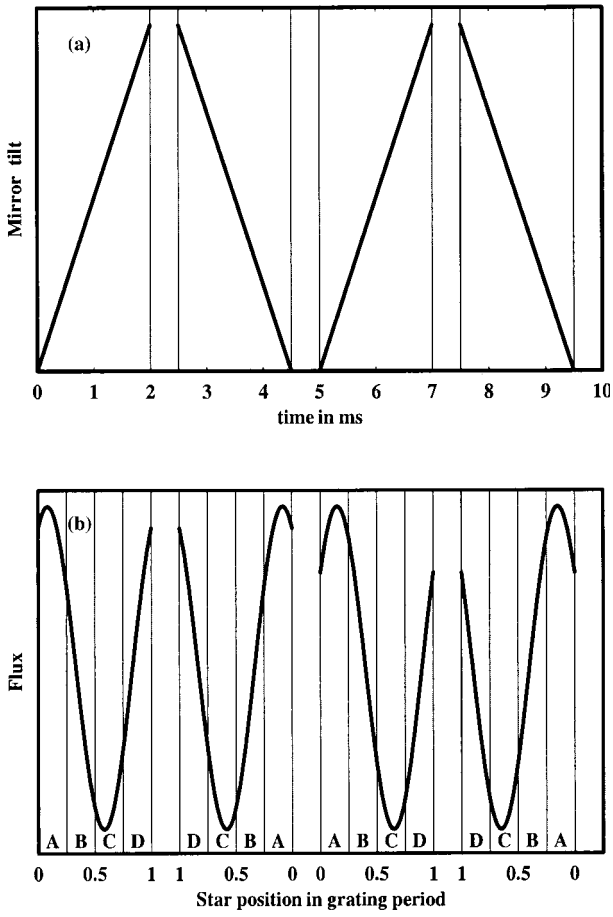

Fig. 1. (b) The signal detected by the GSM photomultiplier corresponds to the transmitted flux of the star image during its displacement on a Ronchi grating. (a) The image position is shifted by means of an oscillating mirror. *A–D*, photon counts integrated over 0.5 ms. The *ABCD* counts for forward and backward scans are averaged to yield the phase shift of the flux sinusoid that corresponds to AA fluctuation.

Image modulation is provided by a galvanometric mirror. The formidable problem of achieving fast and linear response is solved by use of the inertial properties of the oscillating mirror. Modulation is linear to better than 1% and perfectly synchronous in all four modules. During the 5-ms modulation period the forward and backward scans take 2 ms each, and the remaining 2 ms $\times$ 0.5 ms is the dead time

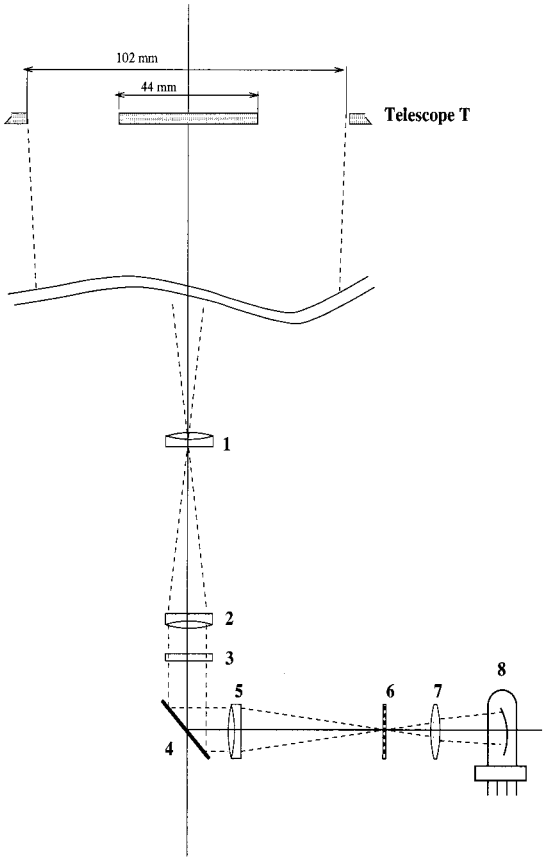

Fig. 2. Optical schematic of a GSM module. The telescope is Maksutov–Cassegrain type with 10-cm diameter: 1, field lens; 2, collimating lens; 3, cylindrical lens; 4, modulating mirror; 5, focusing lens; 6, Ronchi grating; 7, Fabry lens; 8, photomultiplier.

needed for changing the scan direction. Every 5 ms we average the *ABCD* counts for forward and backward scans to compute the phase. Further details can be found in Ref. 10.

The optical layout of the GSM detector box is shown in Fig. 2. A 4-mm aperture in the focal plane of the telescope limits the field to 14 arc min, reducing the contribution of the sky background. A field lens (1) in front of the aperture forms the pupil image near the collimator (2). The parallel beam is deflected by 90° by a modulator mirror (4) and refocused onto the Ronchi grating (6; 40-μm period). A cylindrical lens (3) is located near the collimator to elongate the stellar image along grating lines and thus to reduce the effects of dust particles or grating defects.

In addition to optics, each detector box contains a photomultiplier (8; Hamamatsu R2949), its high-voltage supply, a pulse amplifier and modulation to control circuits. A viewer is used to point and center the star. Typically, a 2^m star gives a count rate of $\approx 6 \times 10^5$ counts/s, and the associated shot noise (see below) is much less than the AA signal.

All four GSM modules receive the same signal, which controls modulation timing. Detected photons are counted at 0.5-ms intervals by the interface board and transferred to PC memory by interrupts. The software provides all necessary functions for instrument testing (e.g., modulation amplitude control and flux measurements) and data acquisition and processing. After the accumulation of data (typically during 120 s), the processing results are shown on the screen and entered into the database.

B. Data Processing

Data (*ABCD* counts) are stored on a computer disk as a sequence of 2-byte integer numbers (16 numbers/5 ms). The parameters of each acquisition and the results of its processing are kept in a separate file that serves as a database. Data processing includes the following steps:

The phases are computed for each channel from Eq. (1), with restoration of the integer numbers of grating periods. In the case of a poor signal-to-noise ratio the phase jumps are successfully removed by a digital filter.

The parabolic trend is fitted and subtracted, leaving only random phase fluctuations. Thus, the GSM can compensate for linear drift of the source during acquisition, which is useful for observations of the polar star without tracking.

The four variances and six covariances of the AA fluctuations, which correspond to all possible combinations of the four modules, are computed. The variances are corrected from the contributions of photon and scintillation noise, as explained below.

The auxiliary quantities, namely, the mean modulation contrast, the mean flux in each module, and its dispersion, are computed as well and provide a measure of the scintillation index.

The last step is the calculation of the AOP of interest, which proceeds in the following way: Fried parameter r_0 is estimated from the AA differential variance[1,11] obtained with modules 1 and 2, which share a common mount. We remove the contribution from noise and apply a correction for a finite exposure time (see below). We also compute the estimates of r_0 from the AA variances obtained with each module. When they are corrected from the effects of the outer scale,[1,13] these variances usually agree well with the differential r_0, ensuring that the AA measurements are not seriously affected by telescope vibrations.

We determine Wave-front outer scale $\mathscr{L}_0$ for each pair of modules by computing the ratio of AA covariance to differential AA variance obtained with modules 1 and 2. These normalized covariances Γ are then compared with the grid of theoretical covariances calculated for various baseline coordinates and values of the $\mathscr{L}_0$ parameter in the von Kármán model.[14] Theoretical Γ are interpolated for the specific value of the baseline (in fact, first a projection of the baseline onto the wave-front plane is computed for the moment of observation from the site and source coordinates), and the appropriate $\mathscr{L}_0$ that fits the measured Γ is found. The value of $\mathscr{L}_0$ that is ultimately adopted is taken as the median of the six

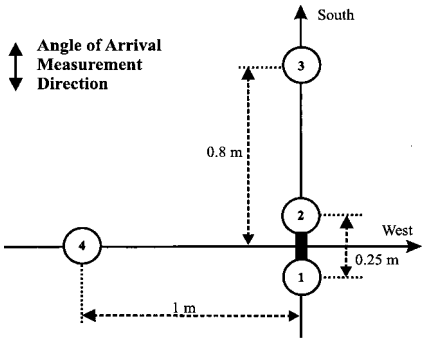

Fig. 3. GSM configuration: Modules 1 and 2 are installed on the same mount and work in a differential mode.

individual values that correspond to the various baselines.

The configuration of GSM modules is shown in Fig. 3. The baseline lengths were chosen for optimal sensitivity of the covariances to the outer scale. Thus the longitudinal baseline is shorter than the transversal baseline because Γ decreases more rapidly in the longitudinal direction than in the transverse one.[6]

Isoplanatic angle θ_0 is calculated from the scintillation index from the formulas given in Section 5 below.

The two-dimensional configuration of the GSM permits the effective wave-front speed to be derived from the temporal cross correlation of AA signals at different baselines. Thus the wave-front coherence time τ_0 can be found. However, this operation is not yet a part of standard signal processing. Examples of the spatiotemporal AA analysis and the problems encountered in estimating τ_0 are discussed in Section 6 below.

3. Error Analysis

In this section we estimate the various sources of error that affect the AOP measurements with the GSM. Most sources of error affect the AA measurements in each module. Let us denote the measured AA signal α. It differs from the atmospheric AA fluctuations α_a by the contributions of several noise sources and can be written as

$$\alpha = \alpha_a + \alpha_p + \alpha_s + \alpha_g + \alpha_m, \tag{3}$$

where α_p is the photon noise, α_s is the scintillation noise, α_g is the modulation noise that arises as a result of the imperfect validity of Eq. (1), and, finally, α_m is the mechanical noise that is due to telescope motion. After considering all these terms, we take into account the error that arises from averaging of α_a during the GSM exposure time of 5 ms. Finally, we estimate the statistical errors of the computed variances and covariances and provide the expressions for the errors of the AOP measured with the GSM.

A. Photon Noise

The numbers of photons A, B, C, and D that enter into Eq. (1) are subject to the statistical fluctuations that are due to the Poisson statistics of the photodetection process. We can safely assume that these fluctuations are uncorrelated. As described in Section 2, the four fluxes A, B, C, and D recorded per modulation can be written as $I_i = N[1 + \gamma \cos(\Phi + \psi_i)]$, where ψ_i are the A, B, C, and D phase shifts that correspond, respectively, to 0, $\pi/2$, π, and $3\pi/2$ and N is the mean count. Assuming that the mean phase Φ is equal to zero, we can write the mean recorded counts as $\bar{A} = N(1 + \gamma)$, $\bar{B} = N$, $\bar{C} = N(1 - \gamma)$, and $\bar{D} = N$.

Differentiating Eq. (1), we relate the photon-noise phase dispersion σ_p (in units of grating period) to the modulation contrast γ:

$$\sigma_p{}^2 = \frac{1}{64N\gamma^2}. \tag{4}$$

To check this expression we performed an experiment in the laboratory that consisted of making measurements without turbulence and using the difference of AA between two modules. A comparison of the values of the differential variance $\sigma_{\text{diff}}{}^2 = \langle(\alpha_1 - \alpha_2)^2\rangle$ and the sum $\sigma_{p1}{}^2 + \sigma_{p2}{}^2$ calculated from Eq. (4) shows that they are within $\pm 5\%$ of each other for various levels of photon flux N and contrast γ.

B. Scintillation Noise

The stellar flux exhibits fluctuations, called scintillation, that are due to atmospheric turbulence.[15] Generally, the scintillation is characterized by an index $\sigma_I{}^2$, defined as the ratio of the flux variance to the square of the mean flux. The scintillation perturbs the *ABCD* counts just as well as the photon noise does and hence is a source of noise in the AA measurements. However, only a specific portion of the scintillation's temporal spectrum contributes to the noise, because fluctuations on time scales longer than 5 ms affect all counts in the same way and do not change the phase. So there is no unique relation between the rms scintillation phase noises σ_s and $\sigma_I{}^2$. The solution to this problem consists in measuring the rapid contrast fluctuations, which are also related to the scintillation noise. As for photon noise, we assume that the scintillation-induced fluctuations of *ABCD* are mutually independent and that their relative rms amplitude is δ ($\sigma_A{}^2/\bar{A}^2 = \sigma_B{}^2/\bar{B}^2 = \sigma_C{}^2/\bar{C}^2 = \sigma_D{}^2/\bar{D}^2 = \delta$). Then, when we take into account both scintillation and photon noises, Eq. (4) becomes

$$\sigma_{ps}{}^2 = \frac{\delta}{64\gamma^2}. \tag{5}$$

Using Eq. (2) to deduce the expression of the dispersion $\sigma_\gamma{}^2$ of the measured contrast and the A, B, C, D mean counts as defined in Subsection 3.A [$\bar{A}^2 = N^2(1 + \gamma)^2(1 + \delta)$, $\bar{B}^2 = N^2(1 + \gamma)^2 = \bar{D}^2$, $\bar{C}^2 = N^2(1 - \gamma)^2(1 + \delta)$] leads to the following expression for δ:

$$\delta = \frac{\sigma_\gamma{}^2}{1 + 0.5\gamma^2}. \tag{6}$$

Instead of using Eq. (4) we can estimate the photon noise from the contrast fluctuations by using Eqs. (5) and (6). This technique also works when both noise sources are present. We have verified in the laboratory (with photon noise only) that, when δ was estimated from the contrast fluctuations by use of Eq. (6), the product δN was within 20% of unity.

In data processing the contrast fluctuations are calculated as one half of the dispersion of the difference of two consecutive contrast values. We implicitly assume that the additional sources of rapid contrast fluctuations (e.g., small-scale turbulence or rapid telescope vibrations) are small; if such is not the case, the photon and scintillation noises are overestimated.

C. Mechanical Errors

1. *Telescope Guiding Errors*

The AA are measured in the declination direction and hence must not be sensitive to guiding errors. However, a small slow component was still present in the signal of some modules; it arose presumably because of the mechanical coupling of telescope motions in hour angles and declination owing to the imperfect worm-gear adjustment. The period of the hour drive worm is 4 min, and in the 2-min standard acquisitions a low-frequency component appears as a half-period of a sinusoid. Fortunately, most of that component is removed when a parabolic trend is subtracted.

2. *Telescope High-Frequency Vibrations*

Telescope high-frequency vibrations are caused by the stepping of the hour drive, which produces a fundamental frequency of 37.5 Hz. Its higher and lower harmonics are also seen in the spectrum of the AA signal. The existence of this vibration was seen during the laboratory tests of the mount made with sensitive accelerometric equipment. However, the total power of the vibrations is negligible compared with the AA fluctuations. Indeed, when those vibrations are removed as a result of the processing by signal filtering the results obtained do not differ by more than their standard errors.

D. Modulation Noise

Modulation noise, i.e., nonsinusoidal signal, nonlinearity of photon counting, errors in modulation amplitude, etc., is the difference between the true and the measured phases that is due to the imperfect validity of Eq. (1). Those errors were discussed extensively by Creath.[12] During the laboratory study the positions of the artificial star on the Ronchi grating were compared with those measured by GSM, and it was shown that the modulation error does not exceed 1% of the grating period.[10] The corresponding error of the AA variance is not greater than 2%.

E. Statistical Noise

The statistical quantities such as AA variance σ_α^2 and covariance C_α are calculated from samples of finite size and hence contain statistical uncertainties. They cannot be computed simply from the sample size because at a sampling rate of 5 ms the individual AA values are not necessarily independent.

1. *Statistical Error of r_0 Estimation*

If the AA measurements are accumulated during a time interval T, the relative error in the differential variance σ_{diff}^2 is given by[16,17]

$$\frac{\delta\sigma_{\text{diff}}^2}{\sigma_{\text{diff}}^2} = \sqrt{2\,\frac{\tau}{T}}. \tag{7}$$

The parameter τ is an equivalent width of the AA correlation, defined as

$$\tau = \frac{1}{[C_{\text{diff}}^2(0)]^2}\int_{-\infty}^{+\infty} C_{\text{diff}}^2(t)\mathrm{d}t, \tag{8}$$

where $C_{\text{diff}}(t)$ is the temporal cross correlation of the AA difference at two apertures i and j (for r_0 measurements $i = 1$ and $j = 2$):

$$\begin{aligned} C_{\text{diff}}(\tau) &= \langle[\alpha_i(t) - \alpha_j(t)]\,[\alpha_i(t+\tau) - \alpha_j(t+\tau)]\rangle \\ &= 2[C_{ii}(\tau) - C_{ij}(\tau)]. \end{aligned} \tag{9}$$

Here $C_{ii}(\tau)$ is the the AA temporal autocorrelation function of the pupil i and $C_{ij}(\tau)$ is the temporal cross correlation of AA at the two apertures i and j; they are defined as

$$\begin{aligned} C_{ii}(\tau) &= \langle\alpha_i(t)\alpha_i(t+\tau)\rangle, \\ C_{ij}(\tau) &= \langle\alpha_i(t)\alpha_j(t+\tau)\rangle. \end{aligned} \tag{10}$$

Using the results of Avila *et al.*,[6] we computed AA difference cross-correlation time τ for the von Kármán turbulence model and the Taylor hypothesis (for a 10-cm circular pupil). The time depends on outer scale $\mathcal{L}_0$, on wind velocity $\mathbf{v}$, and on the baseline. In the case of the La Silla, Chile, GSM campaign ($v \approx 10$ m/s, parallel to the north–south direction, $\mathcal{L}_0 \approx 24$ m, and a baseline of 25 cm), $\tau = 24$ ms. For a GSM integration time $T = 120$ s, the relative error in the AA differential variance is hence equal to 2%, and the statistical relative error of the r_0 estimation ($\delta r_0/r_0 = 3/5\ \delta\sigma_{\text{diff}}^2/\sigma_{\text{diff}}^2$) is equal to 1.2%.

2. *Statistical Error of the $\mathcal{L}_0$ Estimation*

Outer scale $\mathcal{L}_0$ is deduced from the AA normalized covariance Γ.[6] We take into account the statistical errors of both covariance and its normalization factor and arrive at the following formula[16]:

$$\frac{\Delta\Gamma}{\Gamma} = \left(\frac{\tau}{T\Gamma^2} + \frac{\tau_c}{T}\right)^{1/2}, \tag{11}$$

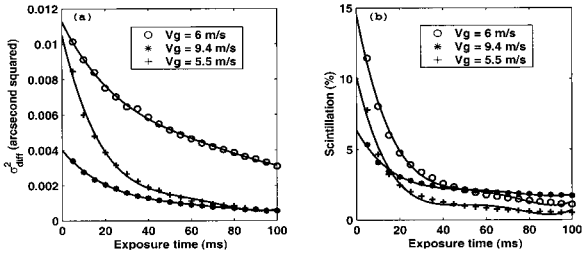

Fig. 4. Effect of the finite exposure time (a) on the measured AA differential variance and (b) on the scintillation index for various wind speeds Vg at ground level. In each case the wind was parallel to the baseline. Data obtained at La Silla Observatory during the campaign of August–September 1997 and binned during processing to increase the exposure time.

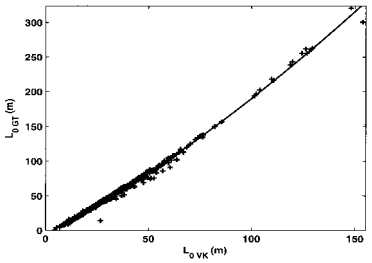

Fig. 5. Effect of the atmospheric turbulence model on $\mathcal{L}_0$ estimation with the GSM. $\mathcal{L}_{0\mathrm{VK}}$ and $\mathcal{L}_{0\mathrm{GT}}$ are the outer-scale values from the von Kármán and Greenwood–Tarazano models, respectively. The data were obtained during the campaign of August–September 1997 at La Silla Observatory.

where τ is defined by Eq. (8). Time constant τ_c is related to the temporal cross correlation $C_{ij}(t)$ of AA at the two apertures i and j defined in Eq. (10):

$$\tau_c = \frac{1}{C_{ij}^{\,2}(0)} \int_{-\infty}^{+\infty} C_{ij}(t) C_{ij}(-t)\mathrm{d}t, \qquad i \neq j,$$
$$i, j = 1, 2, 3, 4. \tag{12}$$

The time constant τ_c was evaluated in the case of the von Kármán model and frozen turbulence (Taylor hypothesis). Indeed, in the study of Avila *et al.*[6] it was shown that this parameter depends on wind speed v, outer scale $\mathcal{L}_0$, and the baseline. In the La Silla campaign, the τ_c values are 108–275 ms for the mean atmospheric conditions (v = 10 m/s and $\mathcal{L}_0$ = 24 m) and a baseline that varies from 25 cm to 1 m. According to Eq. (11) the statistical error of $\mathcal{L}_0$ depends on Γ, so one cannot give its general estimation. Thus, for each particular $\mathcal{L}_0$, we deduce the corresponding error of Γ and consequently of $\mathcal{L}_0$.

F. Exposure Time

During data processing, one can artificially increase the exposure time by binning the data. We used this option to show that temporal averaging for 5 ms has a negligible effect on the computed AA covariances. However, it is important for AA variance and differential variance because their spectra have more power at high temporal frequencies. If this effect is not taken into account it introduces an important systematic bias, increasing the derived r_0 and $\mathcal{L}_0$.

In Fig. 4(a) the dependence of the differential AA variance on exposure time is shown for the three data sets with different ground wind speeds. Smooth curves fitted to the points suggest that we can extrapolate variance σ^2 linearly to zero exposure time:

$$\sigma^2(0\ \mathrm{ms}) = 2\sigma^2\,(5\ \mathrm{ms}) - \sigma^2\,(10\ \mathrm{ms}). \tag{13}$$

This formula is incorporated into the standard data processing, thus eliminating the exposure-time bias.

The frequency bandwidth of stellar scintillation is known to be much higher than that of AA fluctuations. However, the same 5-ms exposure time is used for both quantities. So, as shown in Fig. 4(b), an even higher correction must be applied to the scintillation index. Thus, to avoid this effect of the exposure time, we correct the GSM-measured scintillation index in the same manner as for AA fluctuations [Eq. (13)]. With this correction, the isoplanatic angle deduced from the scintillation index (see Section 5 below) is correctly estimated.

Martin[18] has studied the effect of a finite exposure time to explain the difference between longitudinal and transverse seeing measurements obtained with the differential image motion monitor. We tried to fit the $\sigma^2(t)$ curves with theoretical curves, as suggested by Martin,[18] but with only partial success. The reason is that theoretical curves are computed for a single turbulent layer from Taylor's frozen-turbulence hypothesis, whereas in fact there are usually several layers with different wind speeds and directions.

4. Effect of the Atmospheric Turbulence Model

As explained above, the outer scale $\mathcal{L}_0$ is determined as a parameter of the von Kármán turbulence model[14] that fits the normalized AA covariances. Other models,[19–22] such as the Greenwood–Tarazano[23] model, have been proposed to describe the deviation of the turbulence spectrum from the inertial model of Kolmogorov and Tatarski[15] at low frequencies. Thus the power spectra of the phase shift ϕ introduced by air-index fluctuations that correspond to these models are expressed as

$$W_{\phi,\mathrm{VK}}(f) = 0.0229\, r_0^{-5/3} \left(f^2 + \frac{1}{\mathcal{L}_0^{\,2}}\right)^{-11/6}, \tag{14}$$

$$W_{\phi,\mathrm{GT}}(f) = 0.0229\, r_0^{-5/3} \left(f^2 + \frac{f}{\mathcal{L}_0}\right)^{-11/6}, \tag{15}$$

where f is the spatial frequency. A difference is expected when $\mathcal{L}_0$ is estimated from both models, especially for large outer-scale values. This result is due to a low-frequency extrapolation difference between the two models. We also reduced the data, using the Greenwood–Tarazano model. In Fig. 5 we compare the corresponding outer-scale estimates $\mathcal{L}_{0\mathrm{VK}}$ and $\mathcal{L}_{0\mathrm{GT}}$ for two nights. A very good correlation between these estimates can immediately be seen; a

relation between these two parameters can be represented by a quadratic formula:

$$\mathscr{L}_{0GT} = -5.544 + 1.588\mathscr{L}_{0VK} + 0.0037\mathscr{L}_{0VK}^{2}. \quad (16)$$

One can use this formula to transform the GSM results into the Greenwood–Tarazano model. A more general correspondence between the outer-scale parameters of different turbulence models, as well as the relationship of these wave-front outer scales to the geophysical turbulence outer scale L_0, has yet to be found. However, the $\mathscr{L}_{0VK}$ values provided by the GSM can be used to derive the wave-front statistics, e.g., for optimization of HAR techniques (AO and LBI).

5. Measurement of the Isoplanatic Angle θ_0

The isoplanatic angle θ_0 for AO is given by[24]

$$\theta_0^{-5/3} = 114.7\lambda^{-2}\cos^{-8/3}(z)\int \mathrm{d}h C_N^{2}(h)h^{5/3}, \quad (17)$$

where z is the zenith angle. It was noted in Refs. 24 and 25 that θ_0 can be derived from the scintillation index measured with a 10-cm aperture. We review the associated theory briefly.

The scintillation index σ_I^{2} (flux variance normalized by the square of the mean flux) is related to the $C_N^{2}(h)$ turbulence profile by

$$\sigma_I^{2} = 9.62\lambda^{-2}\int \mathrm{d}h\, C_N^{2}(h)P(h), \quad (18)$$

where λ is the wavelength, h is the altitude, and $P(h)$ is a weighting function that depends on the pupil shape. For a circular pupil of diameter D with a central obscuration ratio ϵ the weighting function is

$$P(h) = \frac{1}{(1-\epsilon^2)^2}\int_0^\infty \mathrm{d}f\, f^{-8/3}\sin^2(\pi\lambda h f^2) \times\left[\frac{2J_1(\pi Df)}{\pi Df} - \epsilon^2\left(\frac{2J_1(\epsilon\pi Df)}{\epsilon\pi Df}\right)\right]^2, \quad (19)$$

where f is the spatial frequency and J_1 is the first-order Bessel function. It was shown in Ref. 15 that, for small D, $P(h) \propto h^{5/6}$, whereas, for large D, $P(h) \propto h^2$. It happens that, for the GSM pupil ($D = 10$ cm, $\epsilon = 0.4$), $P(h)$ is rather close to the $h^{5/3}$ exponent required for measuring θ_0.

Thus we may write $P(h) \approx P(h_0)(h/h_0)^{5/3}$. It follows immediately that

$$\theta_0^{-5/3} = K\sigma_I^{2}, \quad (20)$$

where K is a constant given by

$$K = 11.93\cos^{-8/3}(z)\frac{h_0^{5/3}}{P(h_0)}. \quad (21)$$

The parameter h_0 is defined as the altitude that has the same isoplanatic angle with both Eqs. (17) and (20) with $C_N^{2}(h)$ profiles. Indeed, with Hufnagel's average C_N^{2} profile that corresponds to nighttime conditions[26] and the GSM weighting function, the altitude h_0 obtained is equal to 10 km. This result was confirmed with C_N^{2} profiles obtained with the scintillation, detection, and ranging (SCIDAR) technique on San Pedro Màrtir Observatory, Mexico.[27]

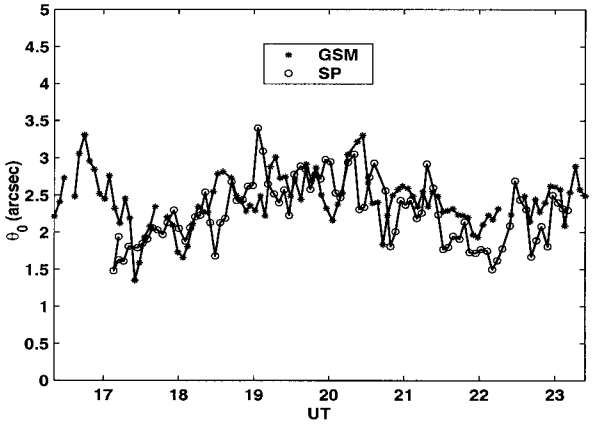

Fig. 6. Isoplanatic angle measurements obtained with the GSM at Maidanak Observatory during the night of 22 July 1998. Measurements of θ_0 (sp) obtained simultaneously with a scintillometer are presented for comparison.

The scintillation index is calculated from GSM data as a normalized dispersion of the sum of *ABCD* counts (such that the flux modulation with the Ronchi grating is canceled). It is corrected for the finite exposure time in the same manner as for the AA variance [Eq. (13)]. Of course, GSM was not originally designed for scintillation measurements. During the Maidanak campaign the scintillation measurements were made simultaneously with a four-channel stellar photometer[28] in the B, V, and R photometric bands with a time resolution of 1 ms. An aperture was exactly the same as that of GSM; stars near zenith were used. One can see from Fig. 6 that there is good agreement between the isoplanatic angles measured with these two instruments, despite a fairly large correction of GSM data for zenith angle (the GSM observed the polar star with $z = 52°$). Thus the isoplanatic angle measurements with the GSM seem to be well validated.

Figure 7 presents the isoplanatic angle measurements for $\lambda = 0.5$ μm obtained during the La Silla campaign. From those measurements one can see that θ has log-normal statistics.

6. Spatiotemporal Analysis

The temporal cross correlation of the AA fluctuations measured with GSM modules i and j separated by a baseline $\mathbf{B}$ is defined as

$$C_{ij}(\mathbf{B}, \tau) = \langle\alpha_i(\mathbf{r}, t)\alpha_j(\mathbf{r}+\mathbf{B}, t+\tau)\rangle, \quad (22)$$

where $i, j = 1, 2, 3, 4$ and $i \neq j$. Assuming that the whole atmosphere is a frozen turbulence moving with a wind speed $\mathbf{v}$ (Taylor hypothesis), the temporal

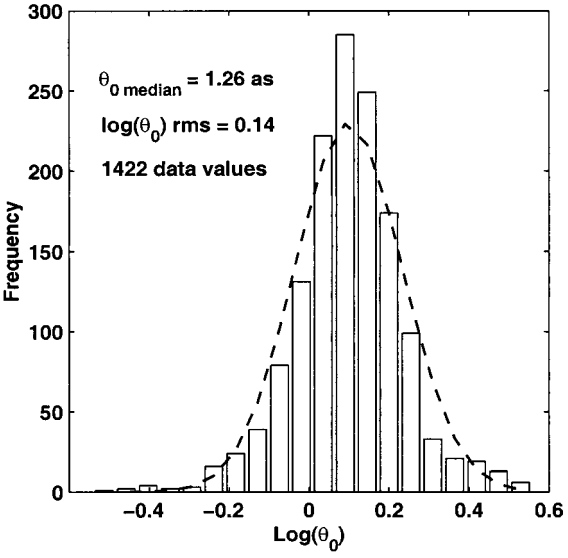

Fig. 7. Distribution of isoplanatic angle θ_0 [in arcseconds (as)] measured with the GSM at La Silla Observatory in August–September 1997. These data are well fitted with a log-normal distribution.

cross correlation in Eq. (22) is reduced to a spatial covariance[6]:

$$C_{ij}(\mathbf{B}, \tau) = C_{ij}(\mathbf{B} - \mathbf{v}\tau). \tag{23}$$

The shape of the cross correlation is characterized by a single peak delayed with $\Delta\tau_{ij}$, which is equal to the transport time of the eddies from pupil i to pupil j. Delay $\Delta\tau_{ij}$ is related to the projection of the wind on the baseline[6,29]:

$$\Delta\tau_{ij} = \frac{B_{ij}\cos(\varphi_{ij} - \eta)}{v}, \tag{24}$$

where B_{ij} is the modulus of the baseline, ϕ_{ij} is its angle relative to the direction of AA measurements, and v is the modulus of the wind speed and η is its direction.

Measurements at two noncollinear baselines (two different φ_{ij}) are necessary for determining the coordinates (v, η) of the wind speed vector. The GSM with six baselines (Fig. 8) offers 11 different $\Delta\tau_{ij}$ measurements (we neglect four baseline pairs, which are parallel or nearly parallel), which are enough to ensure good accuracy of the wind speed determination. Thus the wave-front lifetimes for adaptive optics and Michelson interferometry can be deduced.[30]

Now, in the case of an atmosphere stratified in different turbulent layers, the AA cross correlations display several peaks. Each peak corresponds to a turbulent layer; its localization is related to the layer's wind speed [Eq. (24)], and the height of the peak is related to the energy in this layer. In the case of multilayer turbulence we chose the predominant layer (the highest peak) with which to estimate the wind-speed vector $\mathbf{v}(v, \eta)$.

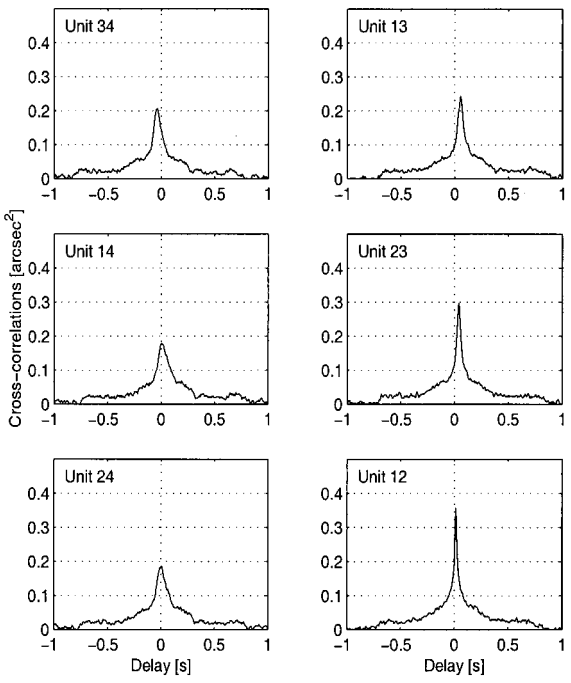

Fig. 8. Examples of temporal cross correlations of AA fluctuations obtained with six GSM baselines at La Silla Observatory (18 September 1997 at 01:38 UT). The turbulent layer wind-speed vector was constructed from the peak positions.

7. Results of the Atmospheric Optical Parameter Measurements with the Generalized Seeing Monitor and $\mathscr{L}_0$ Statistics

Summaries of the campaigns made with the GSM are presented in Table 1. All the atmospheric parameters were calculated for wavelength $\lambda = 0.5$ μm. We draw attention to the larger number of measurements made at La Silla and at Cerro Paranal than at other sites. Also, the mean values of outer scale $\mathscr{L}_0$ at all sites visited are rather similar for different dispersions. The distributions of the AOP, ϵ_0, $\mathscr{L}_0$, and θ_0, are well-fitted by a log-normal law.

The poor seeing (~1.7 arc sec) measured at La Silla was due to the jet stream conditions that prevailed during our mission. The reputation of the sites for good seeing conditions is confirmed, especially for the Maidanak Observatory (0.69 arc sec). From Table 1 one can observe that the correlation between the outer scale and seeing is not significant. Some anticorrelation between the mean seeing and the mean isoplanatic angle (or scintillation) may be noted. However, during the Maidanak campaign the measurements of free-atmosphere seeing were obtained by a new scintillation-based technique[31] and demonstrated that the seeing was dominated by the contribution from the boundary layer.

Figure 9 depicts the $\mathscr{L}_0$ measurements obtained during one night (14 September 1997) at La Silla Observatory. These measurements are presented with error bars estimated in two ways: we obtained the first set of error bars (limited by triangles in Fig. 9) by taking into account all the GSM in-

Table 1. Data Summary of Sites Visited by the GSM[a]

Site	Date	Number of Data	Seeing ϵ_0 (arcsec)	Outer Scale $\mathscr{L}_0$ (m)	Isoplanatic Angle θ_0 (as)	Scintillation Index (%)
La Silla (Chile)	08/26/97	1422	1.64	25.5	1.25	4.61
	09/20/98		(−0.41, ±0.55)	(−10.2, +17.0)	(−0.34, +0.46)	(−1.87, +3.14)
Oukaïmeden (Morocco)	04/10/98	643	1.37	34.2	1.58	3.13
	04/25/98		(−0.41, +0.58)	(−15.6, +28.8)	(−0.49, +0.70)	(−1.43, +2.65)
Maidanak (Uzbekistan)	07/16/98	846	0.69	27.6	2.47	1.48
	07/25/98		(−0.18, +0.24)	(−10.7, +17.5)	(−0.59, +0.77)	(−0.54, +0.84)
Cerro Pachon (Chile)	10/02/98	616	0.89	28.4	2.71	1.27
	10/09/98		(−0.27, +0.39)	(−13.3, +25.0)	(−0.85, +1.23)	(−0.59, +1.10)
Cerro Paranal (Chile)	11/27/98	1884	0.91	23.9	1.91	2.29
	12/20/98		(−0.28, +0.40)	(−11.7, +22.8)	(−0.53, +0.73)	(−0.96, +1.65)

[a]Each campaign is characterized by the mean values (deduced from logarithmic means of the AOP log-normal distributions) of the AOP parameters at $\lambda = 0.5$ μm and at zenith. The values given in parentheses indicate the interval limits, from the mean value, that constitute 68% of each parameter's nightly values ($\pm 1\sigma$ of the log-normal nightly distributions).

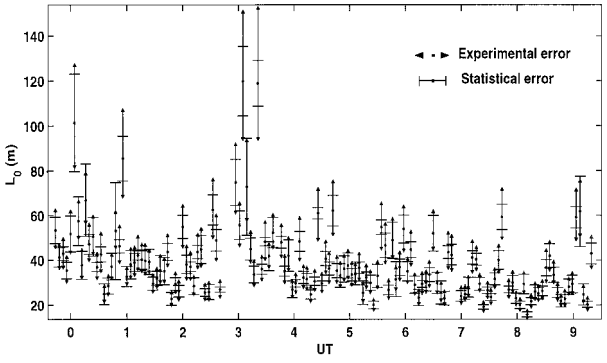

Fig. 9. Outer-scale measurements obtained with a GSM at La Silla Observatory during one night (14 September 1997). The errors in the individual measurements are deduced both from the six baseline statistical rms dispersion and from the GSM global (experimental) error.

strumental errors discussed above. We obtained the second estimate of errors (limited by the bars in Fig. 9) by computing the $\pm\sigma$ uncertainty from the scatter of $\mathscr{L}_0$ at six baselines. One can remark that the instrumental error bars are larger than the statistical ones.

For what we believe is the first time, it is now possible to monitor $\mathscr{L}_0$ with the GSM, to follow its temporal evolution and its changes from one observatory to another. For a duration of one night, $\mathscr{L}_0$ presents decametric values with a log-normal distribution[32] and some bursts that correspond to a newly generated turbulence. These bursts were observed at all sites visited and lasted typically a few minutes. Similar bursts that lasted a few minutes were detected by Avila *et al.*[27] in C_N^2 profiles.

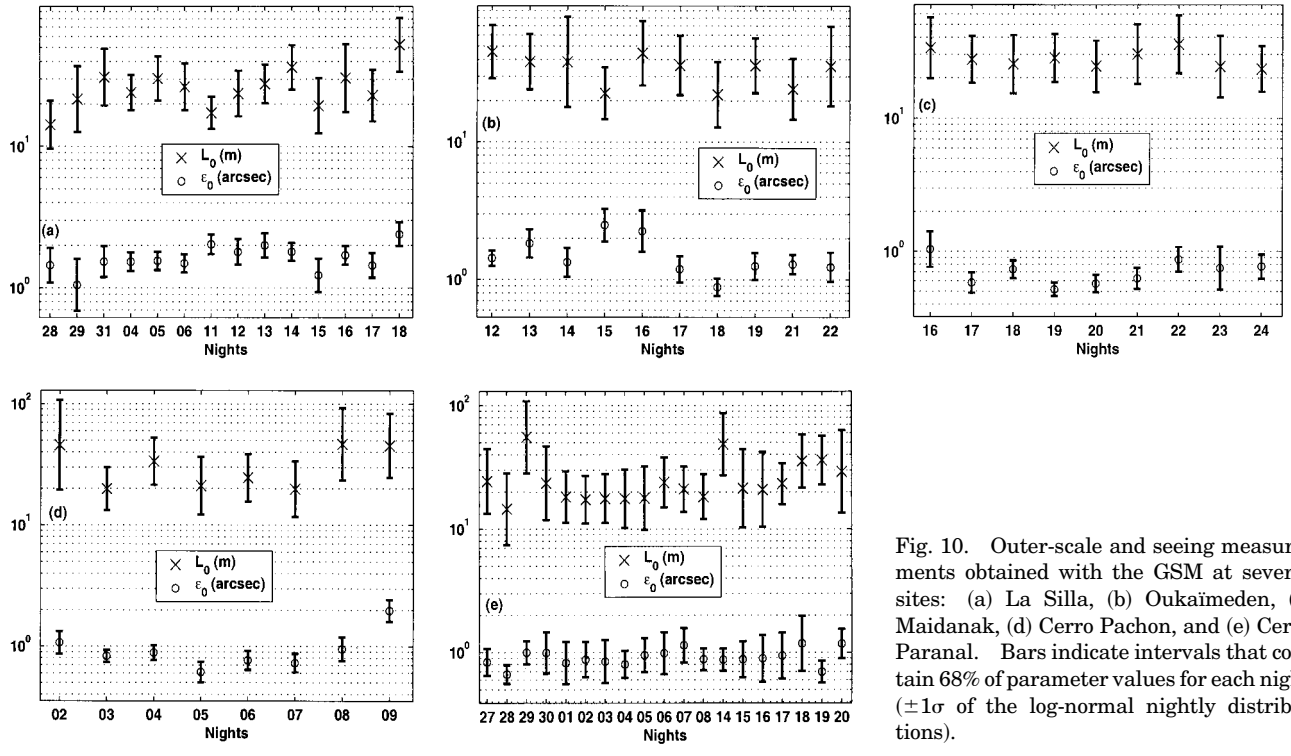

Fig. 10. Outer-scale and seeing measurements obtained with the GSM at several sites: (a) La Silla, (b) Oukaïmeden, (c) Maidanak, (d) Cerro Pachon, and (e) Cerro Paranal. Bars indicate intervals that contain 68% of parameter values for each night ($\pm 1\sigma$ of the log-normal nightly distributions).

We note that during a typical night the $\mathscr{L}_0$ temporal variability is strong, even when bursts are not taken into account. It has been shown that the temporal variability of $\mathscr{L}_0$ is stronger than that of seeing. This means that for optimization of AO systems and LBI observations it would be desirable to monitor the outer scale.

Figure 10 shows the night-by-night evolution of $\mathscr{L}_0$ and ϵ_0 measurements obtained at the various sites visited by the GSM. Each night is represented by the mean values of $\mathscr{L}_0$ and ϵ_0. The bars indicate intervals that contain 68% of nightly values ($\pm 1\sigma$ of the log-normal nightly distributions). One can see that the AOP's have less temporal variability than one-night measurements (Fig. 9).

8. Conclusions

The results presented here show the scope and quality of atmospheric measurements that can be carried out with the generalized seeing monitor. Indeed, for the first time to our knowledge, the wave-front outer scale $\mathscr{L}_0$ was monitored continuously for several nights at a number of astronomical sites. The GSM instrument also provides measurements of seeing ϵ_0, isoplanatic angle θ_0, and the wind speed of turbulent layers (from which the wave-front constant time τ_0 is deduced). Thus the GSM instrument is what we believe to be the first monitor to provide almost complete characterization of astronomical sites for high-angular-resolution techniques.

A quantification of the various error sources of the GSM has been made. Thus we know how accurately the atmospheric optical parameters are measured, and error bars are provided for all GSM data. In addition, the effect of the model that describes the atmospheric turbulence on the wave-front's outer-scale $\mathscr{L}_0$ estimation has been evaluated: The results obtained with the von Kármán and Greenwood–Tarazano models are different but are closely related [Eq. (16)].

The GSM instrument has already produced an important data bank for the major astronomical sites throughout the world: La Silla, Cerro Paranal, and Cerro Pachon (Chile); Oukaïmeden (Morocco), and Maidanak (Uzbekistan). We are now studying all these data to compare the sites, to analyze the temporal evolution of the AOP's, and to investigate their correlations.

References

1. A. Ziad, "Estimation des échelles limites de cohérence spatiale des fronts d'onde et optimisation des observations à Haute Résolution Angulaire en Astronomie," Ph.D. dissertation, (Université de Nice-Sophia Antipolis, Nice, France), 1993.
2. A. Ziad, J. Borgnino, A. Agabi, and F. Martin, "Optimized spectral bandwidth in high angular resolution imaging. Effect of a finite spatial-coherence outer scale," Exp. Astron. **5,** 247–268 (1994).
3. R. Sasiela, *Electromagnetic Wave Propagation in Turbulence. Evaluation and Application of Mellin Transforms* (Springer-Verlag, New York, 1994).
4. D. Winker, "Effect of a finite outer scale on the Zernike decomposition of atmospheric optical turbulence," J. Opt. Soc. Am. A **8,** 1568–1573 (1991).
5. G. Boreman and C. Dainty, "Zernike expansions for non-Kolmogorov turbulence," J. Opt. Soc. Am. A **13,** 517–522 (1996).
6. R. Avila, A. Ziad, J. Borgnino, F. Martin, A. Agabi, and A. Tokovinin, "Theoretical spatiotemporal analysis of angle of arrival induced by atmospheric turbulence as observed with the grating scale monitor experiment," J. Opt. Soc. Am. A **14,** 3070–3082 (1997).
7. C. Coulman, J. Vernin, Y. Coqueugniot, and J. Caccia, "Outer scale of turbulence appropriate to modeling refractive-index structure profiles," Appl. Opt. **27,** 155–160 (1988).
8. J. Borgnino, "Estimation of the spatial coherence outer scale relevant to long baseline interferometry and imaging in optical astronomy," Appl. Opt. **29,** 1863–1865 (1990).
9. V. Lukin, E. Nosov, and B. Fortes, "Effective outer scale of atmospheric turbulence," Opt. Atmosferi **10,** 162–171 (1958).
10. F. Martin, A. Tokovinin, A. Agabi, J. Borgnino, and A. Ziad, "G.S.M.: a grating scale monitor for atmospheric turbulence measurements. I. The instrument and first results of angle of arrival measurements," Astron. Astrophys. Suppl. Ser. **108,** 173–180 (1994).
11. M. Sarazin and F. Roddier, "The ESO differential image motion monitor," Astron. Astrophys. **227,** 294–300 (1990).
12. K. Creath, "Phase-measurement interferometry techniques," in *Progress in Optics*, E. Wolf, ed. (Elsevier, Amsterdam, 1988), Vol. 26, pp. 351–391.
13. J. Borgnino, F. Martin, and A. Ziad, "Effect of a finite spatial-coherence outer scale on the covariances of angle-of-arrival fluctuations," Opt. Commun. **91,** 267–279 (1992).
14. R. Lutomirski and H. Yura, "Wave structure function and mutual coherence function of an optical wave in a turbulent atmosphere," J. Opt. Soc. Am. **61,** 482–486 (1971).
15. F. Roddier, "The effects of atmospheric turbulence in optical astronomy," in *Progress in Optics*, E. Wolf ed., Elsevier, Amsterdam, 1981), Vol. 19, 281–376.
16. J. Bendat and A. Piersol, *Random Data: Analysis and Measurement Procedures* (Wiley-Interscience, New-York, 1971).
17. B. Frieden, *Probability, Statistical Optics, and Data Testing* (Springer-Verlag, Berlin, 1983).
18. H. Martin, "Image motion as a measure of seeing quality," Publ. Astronom. Soc. Pac. **99,** 1360–1370 (1987).
19. A. Consortini and L. Ronchi, "Choice of the model of atmospheric turbulence," Appl. Opt. **5,** 1205–1211 (1972).
20. V. P. Lukin, "Optical Measurements of the outer scale of the atmospheric turbulence," Atmos. Oceanic Opt. **4,** 229–242 (1992).
21. V. P. Lukin, "Intercomparison of models of the atmospheric turbulence spectrum," Atmos. Oceanic Opt. **6,** 628–631 (1993).
22. V. Voitsekhovich, "Outer scale of turbulence: comparison of different models," J. Opt. Soc. Am. A **12,** 1346–1353 (1995).
23. C. Gardner, "Effects of random path fluctuations on the accuracy of laser ranging systems," Appl. Opt. **15,** 2539–2545 (1976).
24. J. Krause-Polstorff, A. Edmund, and L. W. Donald, "Instrument comparison: corrected stellar scintillometer versus isoplanometer," Appl. Opt. **32,** 4051–4057 (1993).
25. G. Loos and C. Hogge, "Turbulence of the upper atmosphere and isoplanatism," Appl. Opt. **18,** 2654–2661 (1979).
26. R. E. Hufnagel, "Propagation through atmospheric turbulence," in *The Infrared Handbook*, W. L. Wolfe and G. J. Zissis, eds. (Environmental Research Institute of Michigan, Ann Arbor, Mich., 1978), pp. 1–6.
27. R. Avila, J. Vernin, and S. Cuevas, "Turbulence profiles with generalized scidar at San Pedro Màrtir Observatory and iso-

planatism studies," Publ. Astron. Soc. Pacific **110,** 1106–1116 (1998).
28. V. Kornilov, "The four-channel stellar photometer with dichroic beam-splitter," Baltic Astron. **7,** 513–524 (1998).
29. R. Conan, A. Ziad, R. Avila, A. Tokovinin, F. Martin, and J. Borgnino, "Spatio-temporal analysis of the wavefront with the GSM," in *Topical Meeting on Astronomy with Adaptive Optics, Present Results and Future Programs*, D. Bonaccini, ed. (European Southern Observatory, Garching-bei-München, Germany, 1998), pp. 133–142.
30. F. Roddier, J. Gilli, and G. Lund, "On the origin of speckle boiling and its effects in stellar speckle interferometry," J. Opt. (Paris) **13,** 263–271 (1982).
31. A. Tokovinin, "A new method to measure the atmospheric image quality," Astron. Lett. **24,** 768–771 (1998).
32. F. Martin, A. Tokovinin, A. Ziad, R. Conan, J. Borgnino, R. Avila, A. Agabi, and M. Sarazin, "First statistical data on wavefront outer scale at La Silla Observatory from the GSM Instrument," Astron. Astrophys. **336,** L49–L52 (1998).